Surface Patch Binding Induced Intermolecular Complexation and Phase Separation in Aqueous Solutions of Similarly Charged Gelatin−Chitosan Molecules

ARTICLE *in* THE JOURNAL OF PHYSICAL CHEMISTRY B · AUGUST 2007

Impact Factor: 3.3 · DOI: 10.1021/jp070745s · Source: PubMed

3 AUTHORS:

Amar Nath Gupta
University of Alberta
16 PUBLICATIONS **198** CITATIONS
SEE PROFILE

Himadri Bohidar
Jawaharlal Nehru University
185 PUBLICATIONS **1,928** CITATIONS
SEE PROFILE

Vinod K Aswal
Bhabha Atomic Research Centre
392 PUBLICATIONS **4,908** CITATIONS
SEE PROFILE

THE JOURNAL OF PHYSICAL CHEMISTRY B

Article

Surface Patch Binding Induced Intermolecular Complexation and Phase Separation in Aqueous Solutions of Similarly Charged Gelatin–Chitosan Molecules

Amar Nath Gupta, H. B. Bohidar, and V. K. Aswal

J. Phys. Chem. B, **2007**, 111 (34), 10137-10145• DOI: 10.1021/jp070745s • Publication Date (Web): 04 August 2007

Surface Patch Binding Induced Intermolecular Complexation and Phase Separation in Aqueous Solutions of Similarly Charged Gelatin−Chitosan Molecules

Amar Nath Gupta and H. B. Bohidar*

Polymer and Biophysics Lab, School of Physical Sciences, Jawaharlal Nehru University, New Delhi-110 067, India

V. K. Aswal

Solid State Physics Division, Bhaba Atomic Research Centre, Mumbai-400 085, India

Received: January 29, 2007; In Final Form: June 19, 2007

The formation of selective surface patch binding induced complex coacervates between polyions, chitosan (cationic polyelectrolyte), and alkali-processed gelatin (polyampholyte), both carrying similar net charge, was investigated for two volumetric mixing ratios: r = [chitosan]/[gelatin] = 1:5 and 1:10. Formation of soluble intermolecular complexes between gelatin and chitosan molecules was observed in a narrow range of pH, though these biopolymers had the same kind of net charge, which was evidenced from electrophoretic measurement. This clearly established the role played by selective surface patch binding driven interactions. The temperature sweep measurements conducted on these coacervate samples through rheology and differential scanning calorimetry (DSC) studies yielded two characteristic melting temperatures located at ≈68 ± 3 °C and 82 ± 3 °C. In the flow mode, the shear viscosity (η) of the coacervate samples was found to scale with (power-law model) applied shear rate ($\gamma^{\bullet}$) as $\eta(\gamma^{\bullet}) \sim (\gamma^{\bullet})^{-k}$; this yielded $k = 0.76 \pm 0.2$ ($1\ s^{-1} < \gamma^{\bullet} < 100\ s^{-1}$), indicating non-Newtonian behavior. The static structure factor ($I(q)$) deduced from small angle neutron scattering (SANS) data in the low q (q is the scattering wavevector) ($0.018\ Å^{-1} < q < 0.072\ Å^{-1}$) region was fitted to the Debye−Bueche regime, $I(q) \sim 1/(1 + \xi^2 q^2)^2$ that yielded a size of $\xi \approx 215 \pm 20$ Å (for r = 1:10) and $\xi \approx 260 \pm 20$ Å (for r = 1:5) samples, implying change in the size of inhomogeneities present with mixing ratio. In the intermediate q region, called the Ornstein−Zernike regime, $I(q) \sim 1/(1 + \xi^2 q^2)$ gave a correlation length of $\xi \approx 10.0 \pm 2.0$ Å independent of the mixing ratio. The results taken together imply the existence of a weakly interconnected and heterogeneous network structure inside the coacervate phase separated by domains of polymer-poor regions.

I. Introduction

Protein−polysaccharide interactions have attracted much attention in the past because of their inherent potential in generating new biomaterials. In addition, such studies provide a basic understanding of the specific and nonspecific interactions operating between complementary polyelectrolytes.[1−6] Normally, polysaccharides are strong polyelectrolytes (PEs), whereas proteins, in addition, can be polyampholytes (PAs). Thus, the problem reduces to that of the general study of interactions between PE and PA biomolecules.[5,6] This can have direct bearing on protein folding, separation and encapsulation, enzymatic immobilization, tissue engineering applications,[7−10] etc. Coacervation is a process during which a homogeneous solution of charged macromolecules undergoes liquid−liquid phase separation, giving rise to a polymer-rich dense phase coexisting with its supernatant. These two liquid phases are immiscible but are strongly interacting. Coacervation has been studied most extensively in aqueous solutions of charged synthetic or biological macromolecules in the last couple of decades. Coacervation has been classified into simple and complex processes depending on the number of participating macromolecules.[6] In simple polyelectrolyte coacervation, addition of salt or alcohol normally promotes coacervation. In complex coacervation, two oppositely charged macromolecules (or a polyelectrolyte and an oppositely charged colloid) could undergo coacervation through associative interactions.[11−19] The charge on the polyelectrolytes must be sufficiently large to cause significant electrostatic interactions but not so large to cause precipitation. It must be noted here that coacervation is not the same as precipitation. The investigation of basic aspects of coacervation of polyelectrolyte complexes provides a foundation not only for the basic understanding of these supramolecular structures but also for their practical applications to protein-related industrial processes. This calls for generating a variety of coacervate materials from biopolymer sources. Since both gelatin and chitosan have found applications in a wide range of product formulations, study of their complex coacervation phenomenon can hardly be stressed.

In the past, all of the coacervation studies on gelatin involved complexation between type-A and type-B, or gelatin and acacia, molecules.[11,13,14] In the Nakajima−Sato model,[15] the theoretical treatment was formalized by inclusion of the solute−solvent interactions in the calculations through Flory−Huggins prescriptions. This model was applied to the data obtained from coacervation of nearly symmetrical poly(vinyl alcohol) molecules of high charge density. A quantitative phase separation condition was proposed by Voorn−Overbeek[16] that related

* Corresponding author. E-mail: bohi0700@mail.jnu.ac.in. Fax: +91 11 2671 7562/ +91 11 2671 7537. Phone: +91 11 2670 4637.

10.1021/jp070745s CCC: $37.00
Published on Web 08/04/2007

polymer charge density and molecular weight to enthalpy of polymer−solvent mixing and Flory−Huggins polymer−solvent interaction parameter. The charge equivalence of the two polyions in the coacervate phase necessitates that the total charge on the protein be the same as the total charge on the complementary polyion. Particularly, for protein−polyelectrolyte systems, this defines the stoichiometry of binding, a condition adequately shown to govern the phase separation in solutions containing human serum albumin and polyelectrolytes.[19] This is supported by the excellent simulation studies carried out by Skepoe and Linse.[3] Interestingly, many examples of non-stoichiometric phase separations involving polyions not having the same charge (polyion charge imbalance) exist.[2] In such cases, the charge imbalance or asymmetry is compensated by small mobile ions (normally the salt).

The phase separation observed in coacervation is driven by the electrostatic and solute−solvent interactions. This results in the gain in configurational entropy and the formation of an amorphous randomly mixed polymer-rich phase remaining in equilibrium with the dilute supernatant. We have provided a rigorous proof[17] to the empirical condition proposed by Dubin et al.,[18] though we deal with a single polyelectrolyte undergoing self-charge neutralization, which is comparable to the complexation between oppositely charged polyelectrolytes described by Dubin et al.[18] The physical condition for phase separation was deduced explicitly for a polyelectrolyte−colloid system having charge density σ and ionic strength I which revealed the relation $\sigma^2/\sqrt{I} \geq$ constant, consistent with experimental observations. A rigorous analysis in the Flory−Huggins lattice model framework yielded a more comprehensive picture of this phenomenon.[17] In the lattice model, r is the number of sites occupied by the polymer having a volume (critical) fraction of φ_{2c}; it was found that phase separation would ensue when $\sigma^3 r \geq (64/9\alpha^2)[\varphi_{2c}/(1-\varphi_{2c})^2]$, which reduces to $(\sigma^3 r/\varphi_{2c}) \geq (64/9\alpha^2) \approx 0.45$ at 20 °C for $\varphi_{2c} \ll 1$, where α is the electrostatic interaction parameter. The separation kinetics was observed to mimic a spinodal decomposition process. Such a model supported generation of a simple coacervate from a homogeneous solution that could be extended to describe phase separation in complex systems too.

Chitosan (poly[β-(1−4)-2-amino-2-deoxy-D-glucopyranose]) is a biodegradable cationic polysaccharide produced by partial deacetylation of chitin derived from naturally occurring crustacean shells. The molecular formula is $C_6H_{11}O_4N$. The polymer is comprised of copolymers of glucosamine and *N*-acetyl glucosamine (see Figure 1). The term chitosan embraces a series of polymers that vary in molecular weight (from approximately 10 000 to 1 million Da) and degree of deacetylation (in the range 50−95%). Chitosan is also found in various fungi. Thus, chitin and chitosan are, at least to some small extent, part of our food supply. Despite its biocompatibility, the use of chitosan in biomedical fields is limited by its poor solubility in physiological media. Chitosan has an apparent pK_a value between 5.5 and 6.5, and upon dissolution in acid media, the amino groups of the polymer are protonated, rendering the molecule positively charged. At neutral and alkaline pH, most chitosan molecules lose their charge and precipitate from solution.[20] Gelatin, a polyampholyte that is obtained from denatured collagen, is a polypeptide with the chemical composition given as follows (as per Merck index): Glycine constitutes 26%, alanine and arginine are in 1:1 ratio and together constitute ≈20%, proline is ≈14%, glutamic acid and hydroxyproline are in 1:1 ratio and constitute ≈22%, aspartic acid ≈6%, lysine ≈5%, valine, leucine, and serine constitute ≈2.0% each, and the rest (1%) is comprised

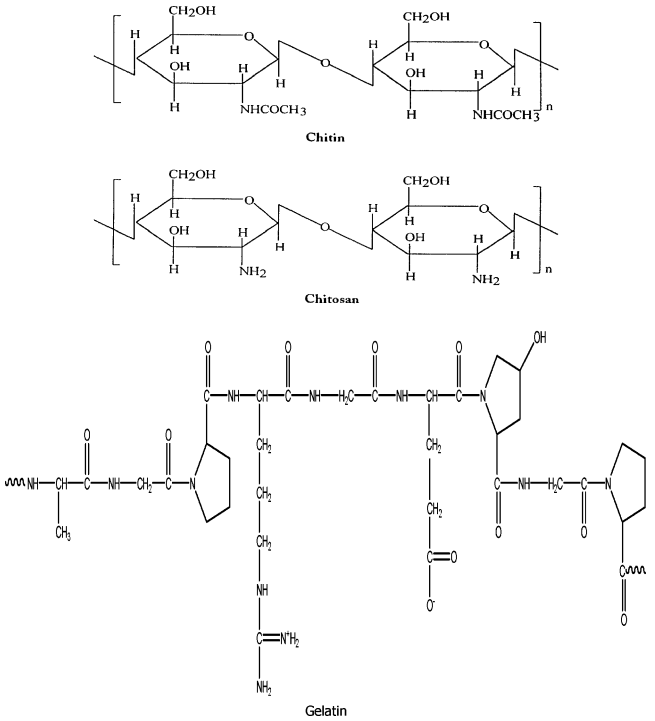

Figure 1. Molecular structures of chitin, chitosan, and gelatin molecules.

of isoleucine and threonine, etc. The aqueous solution properties of gelatin have been well studied and characterized in the past.[21] Depending on the process of recovery, the gelatin molecules bear different physical characteristics. The isoelectric point (pI) of alkali-processed gelatin[22] (type A) is around 9. The hierarchy of length scales existing in gelatin sol, gel, and coacervate phases has been extensively discussed in our earlier work.[23] The molecular structures of chitosan, chitin, and gelatin are depicted in Figure 1.

The microstructure of protein−polysaccharide coacervates, formed of strong electrostatic interactions, has been studied in the past for β-lactoglobulin−gum arabic,[24] whey protein−gum arabic,[25] and β-lactoglobulin−pectin coacervates.[26] The β-lactoglobulin−gum arabic coacervates were found to be associated with vescicular to sponge-like internal structure, whereas the whey protein−gum arabic coacervate was observed to be a highly concentrated (melt-like) phase. In contrast, β-lactoglobulin−pectin coacervates were found to be a heterogeneous phase comprised of pectin networks with protein domains forming the junction points.[26] In the present work, we have shown that the formation of intermolecular soluble complexes and the phenomenon of coacervation can be achieved when a bio-polyelectrolyte (chitosan) interacts with a bio-polyampholyte (gelatin) through surface selective patch binding. In such a process, both of the molecules are associated with the same kind of net charge. The microscopic structures of these coacervates were characterized by small angle neutron scattering (SANS), rheology, and differential scanning calorimetry (DSC), and the results are compared with those of gelatin gels and simple coacervates of gelatin.

II. Materials and Methods

Materials. Gelatin samples of type A (porcine skin extract, bloom strengths = 300, and nominal molecular weights = 100 kDa, isoelectric point (pI) ≈ 9) were obtained from Sigma Chemicals (U.S.A.). Chitosan was bought from Aldrich chemical

company (U.S.A.). The gelatin and chitosan samples were used as supplied. All other chemicals used were of analytical grade, bought from Thomas Baker (India). The solvent used was deionized water; the pH (using 0.1 M HCl or 0.1 M NaOH) and ionic strength of the solvent were first set as per the experimental requirement. The gelatin solutions (0.2% w/v) were prepared by dispersing gelatin in this medium at 50 °C. The macromolecules were allowed to hydrate completely by stirring the solution; this took 1 to 1.5 h. The chitosan solutions were prepared by dissolving 0.2% w/v in 1% aqueous acetic acid solution at 50 °C and stirred well for 2 h to get a homogeneous solution. Both gelatin and chitosan solutions looked optically transparent. For SANS experiment samples were made in D_2O which was used instead of water to obtain better contrast and less background intensity (the large incoherent background is mainly due to the scattering from protons).

Complex coacervate samples were prepared by mixing these two solutions in two volumetric ratios, [chitosan]/[gelatin] = 1:5 and 1:10. The mixture solution was titrated with 0.1 N NaOH to increase the pH, and the cloudiness was monitored through turbidity measurements. The turbid samples were subjected to centrifugation at 10 000 rpm for 30 min, which separated the turbid solution into two liquid phases, namely, the coacervates at the bottom and supernatant at the top. The polymer-rich phase at the bottom was collected after decanting the supernatant. This was repeated at least three times, which yielded the coacervates. This is the normal procedure of extracting the coacervate from the reacted solutions.[27−30] These coacervate samples were analyzed by SANS, rheology, and DSC to probe their thermal and micro-structural properties.

III. Results and Discussion

(a) Phenomenology of Coacervation. The phenomenology of the formation of intermolecular aggregates depends on the physical environment of the polymer chains in the solution. Thus, the solution pH, ionic strength, temperature, polymer charge density, and polymer mixing ratio all play a significant role. As has already been mentioned, intermolecular complex formation is an associative interaction involving electrostatic forces (includes surface selective patch binding interactions). Thus, it was imperative to begin such studies with probing of the electrophoretic properties of the biopolymers involved.

(i) Electrophoresis Studies. Electrophoretic mobility measurements were performed on chitosan and gelatin (0.2% w/v each) samples. The instrument used was a Zeecom-2000 (Microtec Corporation, Japan) zeta-sizer that permitted direct measurement of electrophoretic mobility and its distribution. In all of our measurements, the migration voltage was fixed at 25 V. The instrument was calibrated against 10^{-4} M AgI colloidal dispersions. The first objective was to ascertain the zeta potential of chitosan and gelatin samples separately. The data are shown in Figure 2 which implies that zeta potential is positive for chitosan molecules regardless of the solution pH; this proves the cationic nature of chitosan. The zeta potential was ≈40 mV for pH 4 which decreased to almost zero for the pH 7.0 sample where significant loss of solubility was observed. On the other hand, the zeta potential profile for gelatin reveals a clear isoelectric pH, pI ≈ 9.0, consistent with its nominal definition. Gelatin is a low charge density polyampholyte, as is unambiguously seen from Figure 2. The zeta potential of this biopolymer was ≈10 mV for pH 4 which decreased to ≈ −5 mV for pH 10 solution. To a good approximation, it can be presumed that zeta potential is directly proportional to the net charge on the particle if one assumes that the particles are non-free-draining.

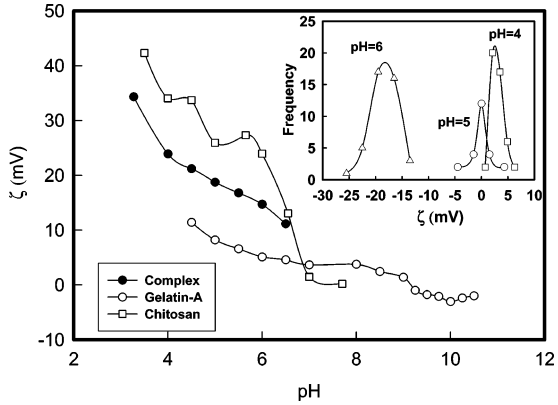

Figure 2. Variation of zeta potential as a function of solution pH for gelatin, chitosan, and the coacervating solution (r = 1:10). Notice that the zeta potential value of the soluble complex lies in between that of gelatin and chitosan for all solution pHs. The data clearly reveal the charge neutralization produced due to intermolecular binding between the two biopolymers. The inset shows the charge distribution of gelatin type-B molecules (pI ≈ 5) as function of pH included for comparison.

The zeta potential data for the soluble complexes are shown in Figure 2 for comparison, and these data lie comfortably between the high charge density chitosan and low charge density gelatin data. It means that there is an intermolecular charge neutralization mechanism involved that has resulted in producing these complexes bearing intermediate charge. Complex formation and coacervation was observed in the pH range where the two biopolymers had the same type of net charge, which indicates anomalous binding behavior between the two biopolymers. This can be attributed to the phenomenon of surface selective patch binding between gelatin and chitosan molecules which will be discussed later.

(ii) Turbidimitric Titration. The simplicity and sensitivity of the turbidimitric titration method as applied to protein−polyelectrolyte systems are based on the fact that turbidity is proportional to both the molecular weight and the number density of particles present in a dispersion. The turbidimitric titration experiments were performed using a colorimeter (model-910, Brinkmann Instruments, U.S.A.) operating at a wavelength of 450 nm; details are given elsewhere.[30] The change in turbidity mirrors the extent of interactions between the two biopolymers (gelatin and chitosan) prevailing at an instance. For titration, chitosan (0.2% w/v) and gelatin solutions (0.2% w/v) were mixed in the ratios r = 1:5, 1:10, 1:15, and 1:20. Typically, a mixed solution was kept on a magnetic stirrer, and was stirred at moderate speed with stir bars. Such a solution was titrated with a 0.1 M NaOH base, and the transmittance and pH changes of the mixture were noted throughout. We observed the first occurrence of turbidity corresponding to the formation of soluble complexes that was measured (pH_c). The titration process was continued until maximum turbidity (pH_ϕ) was noticed (formation of insoluble complexes). The titration profiles are shown in Figure 3 for various mixing ratios of gelatin and chitosan. These transition pHs have been well defined and discussed, in general, for coacervating systems in detail in the past[12,28−30] for other complex coacervates. The soluble complexes could be formed in a very narrow range of pH. At pH_c, the initiation of intermolecular soluble aggregate formation comprising charge neutralized chitosan−gelatin complexes ensues. Eventually, these lead to the formation of microscopic coacervate droplets which in turn coalesce through Ostwald ripening to minimize the surface free energy and macroscopic droplets are generated. In this process, the growth of larger droplets at the expense of smaller ones is facilitated

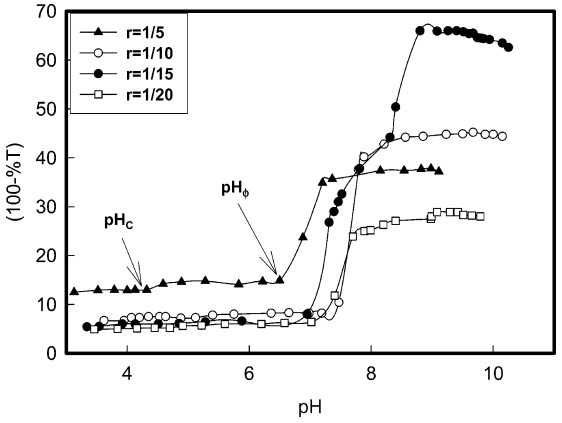

Figure 3. Titration profile of gelatin−chitosan solution as a function of pH for varying mixing ratios of the coacervating solution. Experiments were performed at room temperature (20 °C); turbidity measurements correspond to the wavelength 450 nm. Notice that change in pH_c is not clearly discernible, while pH_ϕ is observed to shift to lower pH values as r is increased.

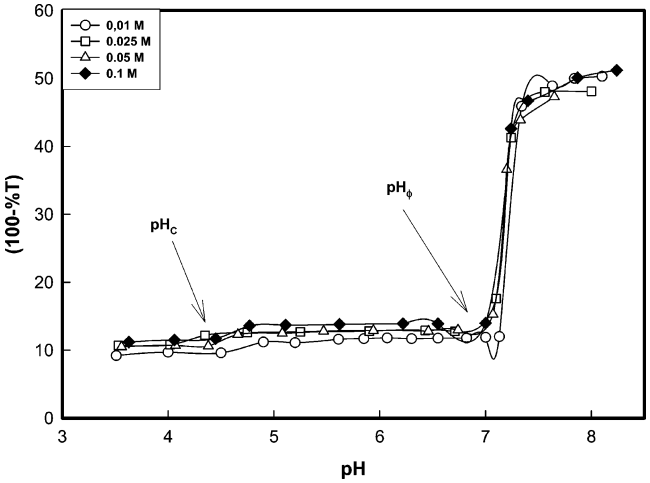

Figure 4. Titration profile of $r = 1{:}10$ gelatin−chitosan solution as a function of pH for varying ionic strengths of the coacervating solution. Experiments were performed at room temperature (20 °C); turbidity measurements correspond to the wavelength 450 nm. Notice that change in pH_c is not clearly discernible, while pH_ϕ is observed to shift to lower pH values as the salt concentration is increased.

(Laplace pressure effect, $\Delta P = 2\gamma/R$, where R is the size of smaller droplets and γ is the surface tension).

Normally, for pH > pH_ϕ, one observes the formation of large insoluble complexes that undergo precipitation immediately, which is observed in the turbidity−pH profile as a sharp drop in measured turbidity values.[12,28−30] In the present case, it was observed that for pH > pH_ϕ the turbid solution did not undergo precipitation instantaneously, and we found a flat or saturated type of curve extending beyond the maximum turbidity pH, but the precipitation started within a few hours. This can be explained in the following way. Initially, the size of the insoluble aggregates was small which was not conducive for instantaneous precipitation. These aggregates grew to a larger size with time, and eventually precipitation ensued. The insoluble complexes were not amenable to electrophoresis measurements because these dispersions sedimented gradually. At pH_ϕ, a binding saturation was reached that was dictated by the stoichiometry of the polymers involved.

Figure 3 clearly implies the shifting of pH_ϕ from ≈7.2 for $r = 1{:}20$ to ≈6.5 for $r = 1{:}5$. However, the variation in pH_c values was less discernible. The formation of the insoluble aggregates was taking place at much lower pH values when the mixing ratio was increased. The electrophoretic data clearly indicated the variation of gelatin charge density with pH which ought to influence intermolecular binding. This, however, does not change the overall picture of coacervation. It affects the degree of charge neutralization in a coacervate solution only. As the value of the chitosan-to-gelatin ratio decreases (abundance of gelatin), charge neutralized soluble complexes could be formed at high pH. This can be qualitatively understood from the fact that when there is a propensity of positively charged segments, one needs a large amount of negative charge on each gelatin molecule (high molecular charge density) to achieve charge neutralization, and this can be realized at high pH. The ionic strength dependence of these transition pHs was measured (see Figure 4); an invariance was clearly seen as far as the pH_c value, but subtle changes in pH_ϕ values were concerned. This indicated that the intermolecular interactions were poorly screened by mobile ions. Regardless, the presence of salt ions was necessary to compensate for the charge imbalance present in the soluble complexes and achieve charge neutralization. The ability of the system to undergo coacervation transition in the absence of salt implies that the two biomolecules followed a symmetric binding character as far as the stoichiometry was concerned. At this stage, it would be improper to comment more on this.

(iii) DLS and Viscometry Studies. The coacervating solution was subjected to dynamic laser light scattering and viscometry studies to map the growth of soluble intermolecular complexes as a function of pH change. Dynamic light scattering (DLS) experiments were performed (scattering angle = 90°, laser wavelength = 632.8 nm) on a 256-channel Photocor-FC (Photocor Inc., U.S.A.) instrument that was operated in the multi-tau mode (logarithmically spaced channels). During the titration process, a few milliliters of the sample was drawn from the reaction beaker and loaded into a borosilicate cylindrical cell (volume =5 mL) and DLS experiments were performed. The data were analyzed both in the CONTIN regularization and in discrete distribution modes (multiexponential). The CONTIN software generates the average relaxation time of the intensity correlation function, which is solely related to the Brownian dynamics of the diffusing particles for dilute solutions. The intensity correlation data were force fitted to a double-exponential function without success. Thus, we have relied on a single-exponential fitting (with polydispersity) and the chi-squared values were >90% consistently for all of the correlation data. This yielded the apparent translational diffusion coefficient values. Correspondingly, the apparent hydrodynamic radii (R_h) of the particles, at room temperature (20 °C), were determined from knowledge of the translational diffusion coefficient (D_T). These values were used in the Stokes−Einstein equation, $D = k_BT/f$, with the translational friction coefficient being $f = 6\pi\eta_0 R_h$, where k_B is the Boltzmann constant and η_0 is the solvent viscosity. The data analysis revealed apparent particle sizes in the pH range pH_c to pH_ϕ. Particles of an apparent size of ca. 280 nm were observed at pH ≈ 4 (Figure 5 (point A)), which owe their origin to the ensemble of noninteracting or weakly interacting gelatin and chitosan molecules. Gelatin is associated with a radius of[21] ≈35 nm, and chitosan being a polyelectrolyte can have a size that is much bigger (≈280 nm). In light scattering experiments, the measured size is biased toward the particles of higher size. The linear charge density of chitosan decreases due to charge neutralization at the binding site as gelatin binds to chitosan. This will increase the flexibility of the gelatin bound chitosan complex vis-à-vis that of a free chitosan molecule. Thus, the ensemble of scattering particles

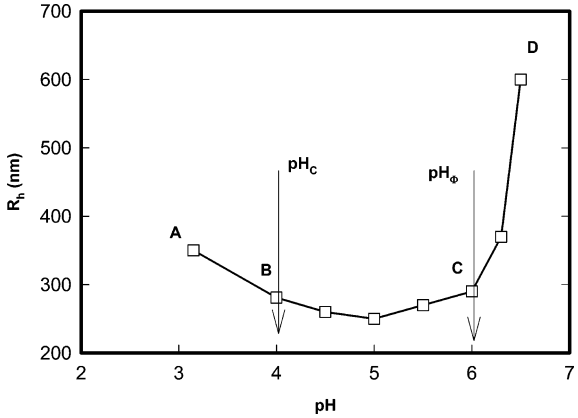

Figure 5. Variation of apparent Stokes radius with pH of the soluble complexes (r = 1:10), measured at 20 °C. Apparent Stokes radius of chitosan (A), intermolecular soluble complexes (B and C), and intermolecular insoluble complexes and clusters (D) are shown. It was noticed that the size decreased with pH, indicating that binding of gelatin to chitosan produces intermolecular complexes of apparent size much less than that of chitosan. The pH_c and pH_ϕ values observed from DLS data are lower than those obtained from turbidity data by a factor of half pH units. See text for details.

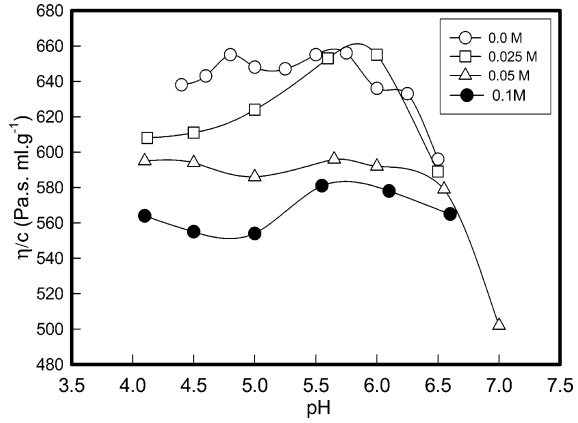

Figure 6. Specific viscosity (η/c) of soluble complexes as a function of pH and ionic strength of the coacervating solution. Rheology data pertain to the flow mode measurements where a fixed shear rate (1 s^{-1}) was used, and experiments were performed at 20 °C. See text for details.

in the solution with pH > pH_c will have fewer particles with large size and the apparent size will, therefore, reduce. This is clearly manifested in Figure 5 (points B and C). These soluble complexes become larger in size as the pH approaches pH_ϕ, and in addition, such complexes fuse to yield large aggregates which ultimately generate coacervate droplets (Figure 5 (point D)). It has been argued earlier that between pH_c and pH_ϕ such binding becomes strongly cooperative.[27−30]

Specific viscosity measurements were performed on the same coacervating solutions at different pHs. The instrument used was a sine wave (30 Hz) vibro viscometer SV-10 model manufactured by A & D company Ltd (Japan). The specific viscosity was seen to increase as the solution pH increased from 4 to 6, implying the formation of intermolecular complexes of higher size. The data are plotted in Figure 6. The data clearly indicate occurrence of maximum binding close to pH ≈ 6, where large soluble complexes are present in abundance. Beyond this pH, large insoluble complexes are formed that sediment gradually, which can be compared to the turbidity plateau seen in Figures 3 and 4. A second observation pertains to the decrease in the specific viscosity value with ionic strength of the solution for a given pH which is indicative of the existence of smaller soluble complexes in higher ionic strength solutions. Thus, the coherent picture that emerges from DLS, turbidity, and viscosity data is that soluble complexes are formed in the reacting solution (at $pH_c \approx 4.5$) and their size and number increase as the pH approaches $pH_\phi \approx 6.5-7.5$.

(iv) Surface Selective Patch Binding. A comparison of the turbidity and electrophoresis data presented (Figures 2 and 3) unambiguously illustrates that the pH_c and pH_ϕ values were much less than the pI = 9 value of gelatin. Also, chitosan was observed to be cationic in the pH range 4−8. Thus, the binding was observed between two biopolymers having the same kind of net charge. In addition, the binding behavior exhibited ionic strength dependence, indicating an electrostatic nature of the forces involved (Figure 4). Such bindings are often referred to as binding on the wrong side of the pH. This type of anomalous binding has been observed in a variety of systems which is well documented in the literature.[31−33] Surface patch controlled attractive electrostatic interactions between proteins and adsorbent having the same net charge were studied, by ion-exchange chromatography (IEC), for lysozyme, ribonuclease A, cytochrome-*c*, and α-chymotrypsinogen systems, and it was observed that such interactions were governed by the characteristics of the solvent medium like the pH, ionic strength, etc.[31] The "retention maps" for the pH dependences of IEC capacity factors were quite revealing. It clearly established the existence of patch binding without a doubt. This was attributed to the heterogeneous charge distribution on the protein surface that facilitates binding, though the net charge on protein may be of the same kind as that of the absorbent.

In a more detailed and quantitative experiment, the intermolecular binding between the selected proteins RNAse, lysozyme, and bovine serum albumin (BSA) and polyelectrolytes with varying linear charge densities was studied by DLS and turbidimetry.[32,33] These results supported the conclusions of retention maps constructed and reported by Regnier et al.[34] It was also shown that the persistence length of the polyelectrolyte plays a very important role in the binding process. Namely, the higher the flexibility, the greater the extent of binding. An approximate model for quantitative estimation of charge on the soluble complexes, both at pH_c and pH_ϕ, was proposed which did imply charge neutralization due to surface patch binding. This model assumed that the protein molecules were non-draining in both electrophoresis and DLS studies; thus, it could be argued that the translational friction experienced by these molecules can be assumed to be identical in both cases.

However, a flexible polypeptide like gelatin cannot be expected to follow the above-mentioned prescription. Such molecules are nondraining in DLS and free-draining in electrophoresis experiments.[35] This does not allow the analysis of our experimental data in the Gao et al. framework.[32] Regardless, the qualitative features observed by Regnier et al.,[34] Gao et al.,[32] and Park et al.[33] are clearly visible in the intermolecular complexation data presented here. These can be summarized as follows: (i) formation of intermolecular soluble complexes was observed with both biopolymers having the same kind of net charge, (ii) the soluble complex is, actually, the partially charged neutralized polyion (chitosan), and (iii) the interaction is electrostatic and is site specific.

Gelatin is a low charge density polyampholyte. It must be realized that the gelatin molecules do carry positively and negatively charged segments at all pHs, though at some pHs there is excess of one type of charge. The charge distribution has been explicitly shown in the past for gelatin molecules as a function of pH which is reproduced in the inset of Figure 2.

Though the molecular charge heterogeneity is not obvious from this plot, regardless, it reveals the shift of the net charge distribution with pH for this polyampholyte molecule rather clearly. The soluble complex had a zeta potential of ≈35 mV at pH 4 (close to pH_c) that reduced to ≈10 mV at pH_ϕ. Corresponding values for chitosan are ≈45 and 12 mV, respectively. This implies that the selective surface patch binding with gelatin has resulted in the formation of a gelatin−chitosan complex that had much less charge than the polyelectrolyte. Beyond pH ≈ 7.5, both the chitosan and soluble complex solutions underwent precipitation. The data at hand do not permit us to discuss the patch binding aspect further without avoiding speculation. Second, for the same reason, it will be inappropriate to draw conclusions about the role played by non-electrostatic interactions in our system.

(b) Microstructure of Coacervates. Understanding the physical structure of the coacervate phase on microscopic length scales is extremely important. This polymer-rich phase is biphasic in nature with the solvation water present either as interstitial bulk or as water bound to the strongly interacting biopolymer chains. It has been shown recently that these chains dissipate energy to the environment only via the surface of coacervate, whereas, in the bulk, these chains exchange energy with each other with negligible or no dissipation.[36] It is also appropriate to compare the structural properties of gelatin−chitosan coacervates with those of gels and coacervates made of gelatin molecules.

(i) SANS Studies. SANS is an extremely sensitive diffraction technique, which involves scattering of a monochromatic beam of neutrons from the sample and measuring the scattered neutron intensity as a function of the scattering angle. Our experiments were performed on the spectrometer at the G. T laboratory, Dhruva reactor (Bhaba Atomic Research Centre, Trombay, India).[37] The wavelength of the neutrons used covered the scattering vector (q) range (in single detector setting, see ref 37 for details)

$$7 \times 10^{-3}\ \text{Å}^{-1} \leq q \leq 3 \times 10^{-1}\ \text{Å}^{-1}$$

where $q = (4\pi/\lambda) \sin \theta/2$, λ is the wavelength of the neutron, and θ is the scattering angle. The dense polymer phase coacervate was transferred to a quartz cell with a thickness of 2 mm, and scattered intensity was measured as a function of scattering vector. The measured intensity was corrected for the background and the empty cell contribution, and the data were normalized to get the structure factors. The raw data were corrected for background, sample cell, and electronic noise by conventional procedures. Furthermore, the two-dimensional isotropic scattering data were azimuthally averaged. This was converted to an arbitrary unit scale using the incoherent scattering data of pure water (see ref 38 for details).

The differential scattering cross section, $d\Sigma/d\Omega(q)$, from a collection of scattering particles consists of two terms, the first of which depends on the intraparticle scattering (denoted as $P(q)$, depends on the shape and size of the particle, and in principle can be calculated for any geometry) and the second, on the interparticle scattering (denoted as $S(q)$, depends on the correlation between the spacing of the particles and their orientations). Basically, $P(q)$ and $S(q)$ are intra- and interparticle structure factors. The scattering cross section is written as

$$d\Sigma/d\Omega(q) = kP(q)\,S(q) \tag{1}$$

Here, k is a constant term that depends on the contrast factor, number of particles per unit volume of the sample, and average volume of the single particle. The concept remains invariant by substituting the differential scattering cross section, $d\Sigma/d\Omega(q)$, with $I(q)$, which is the measured scattering intensity. For a diluted solution, the interparticle structure factors are $S(q) = 1$ and the scattering intensity is governed by $P(q)$.

SANS data were analyzed, in random phase approximation (see ref 23 for an extensive discussion), in two ranges of scattering vectors: low q range (Debye−Bueche model)[39] and intermediate q range (Ornstein−Zernike model).[40] Analysis of SANS data within the model of mean field theory reveals that for the polymers in good solvent, at equilibrium, the structure factor of concentration fluctuations at intermediate wavevector, known as the Ornstein−Zernike (O−Z) function, is given by

$$I(q) = I(0)/(1 + q^2\xi^2); \qquad q\xi \ll 1 \tag{2}$$

where $I(0)$ is the extrapolated structure factor at zero wave number and ξ is the correlation length or mesh size of the network. An "excess scattering" has been reported at low wave-numbers from polymeric solutions caused by enhanced long-wavelength concentration fluctuations in these systems. It is not clear so far as to what causes this excess scattering. However, Koberstein et al.[41] have suggested long-range random inhomogeneities with correlation length many times larger than the radius of gyration of the dissolved polymer to cause this excess scattering. If the spatial scale of density fluctuations due to the presence of inhomogeneities is large when compared with the correlation length (ξ), then the two contributions can be treated separately and added to give the total structure factor as

$$I(q) = I_L(q) + I_{ex}(q) \tag{3}$$

where $I_L(q)$ is the Ornstein−Zernike (O−Z) function, and the Debye−Bueche (D−B) structure factor has the form $I_{ex}(q)$ given by

$$I_{ex}(q) = I_{ex}(0)/(1 + q^2\zeta^2)^2 \tag{4}$$

where $I_{ex}(0)$ is the extrapolated structure factor at zero wavevector. Fitting of experimental SANS data (which is a smooth curve, not shown) to eq 3 required that the low and high q domains were separated reliably. Normally, the D−B region contains substantial data fluctuation that gives an impression that at the crossover from the O−Z to D−B domain there is a sharp discontinuity with the tail end of the O−Z zone, showing pronounced ghost data points in the $1/I(q)$ versus q plot. This is clearly manifested in Figures 7 and 8. A least-squares fit of the structure factor data in the low q range, $0.018\ \text{Å}^{-1} \leq q \leq 0.072\ \text{Å}^{-1}$ (see Figures 7 and 8), to the D−B function yields the size of the heterogeneities ($\zeta = 215 \pm 20$ Å for $r = 1{:}10$ and $\zeta = 260 \pm 20$ Å for $r = 1{:}5$) present inside the coacervate phase. Second, the measured correlation length (Figures 7 and 8) determined by fitting high q region data to the O−Z function gave $\xi = 10.0 \pm 2.0$ Å for both the $r = 1{:}10$ and $r = 1{:}5$ samples, which is much smaller than the persistence length of gelatin, which is ≈25 Å. For gelatin coacervates, gels, and sols, the correlation length values reported[23] are 12, 26, and 26 Å, respectively (see Table 1). The size of the heterogeneities reported for such systems was ≈200 Å which is comparable to the size of the heterogeneities, $\zeta = 215 \pm 30$ Å and $\zeta = 260 \pm 20$ Å, reported now. Thus, it can be inferred that the simple and complex coacervates of gelatin bear identical structural signatures. Coacervates are strongly interacting intermolecular complexes that exhibit heterogeneous microstructure.[27,28] In addition, the presence of nonequilibrium effects contributes to

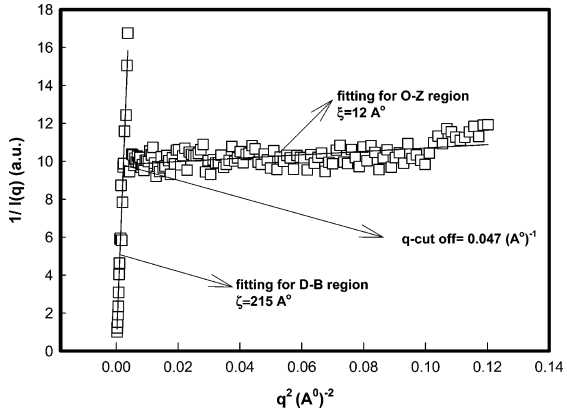

Figure 7. SANS data for the $r = 1{:}10$ sample taken in deuterated water at 20 °C. Length scales like inhomogeneity size (ζ) and mesh size (ξ) were calculated in the O−Z regime and D−B regime, respectively, through fitting of the data to eqs 2 and 4. The q cutoff clearly distinguishes the two regions.

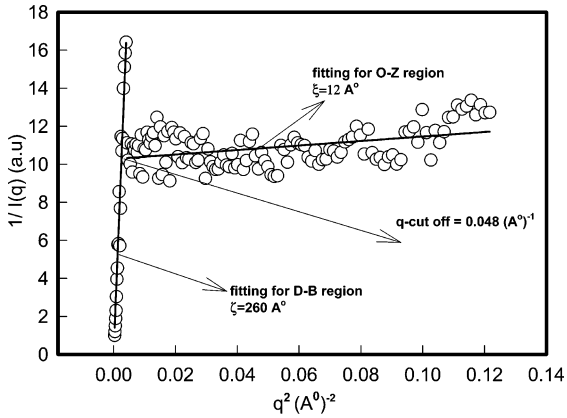

Figure 8. SANS data for the $r = 1{:}5$ sample taken in deuterated water at 20 °C. Length scales like inhomogeneity size (ζ) and mesh size (ξ) were calculated in the O−Z regime and D−B regime, respectively, through fitting of the data to eqs 2 and 4. The q cutoff clearly distinguishes the two regions.

the microphase separations, and creation of local inhomogeneities which has been discussed in detail earlier.[23]

(ii) Rheological Studies. Rheology experiments were performed using an AR-500 model stress controlled rheometer (T.A. Instruments, U.K.) with the objective to inter-relate the stiffness and thermal stability of the network in flow, frequency sweep, and temperature sweep modes. The dynamic rheology of the solutions was measured using a stainless steel cone-plate geometry with a radius of 60 mm, an angle of 2°, and a truncation gap of 58 μm, whereas gels and coacervates were studied by using a parallel-plate geometry with a radius of 20 mm and a truncation gap of 500 μm. The truncation gap was deliberately chosen to be more than the length scales existing in coacervates. In temperature ramp measurements, the temperature was increased at the rate 3 °C/min. Silicon oil was used as a solvent trap to prevent loss of solvent because of evaporation. The shear induced flow behavior of coacervate samples was quite revealing. The shear rate dependent viscosity data of these samples are plotted in Figure 9, which reveals the non-Newtonian yield.[42] In addition, shear-thinning behavior was exhibited by these samples. The data presented in Figure 9 clearly identified the region where the power-law model[42] adequately described the fitting

$$\eta(\gamma^{\bullet}) \sim (\gamma^{\bullet})^{-k} \tag{5}$$

with $k = 0.76 \pm 0.2$ for $1\ s^{-1} < \gamma^{\bullet} < 100\ s^{-1}$. In fact, k reveals the viscous response of the samples to applied shear: $k = 0$ gives Newtonian, $k < 0$ indicates shear thickening, and $k > 0$ implies shear-thinning behavior. Thus, shear-thinning features are clearly manifested in these samples. The drop in the viscosity value observed at higher shear rate could correspond to the shear induced rupture of the weak network structures present in the system. Preferential alignment of these networks along the direction of applied shear can have a similar effect.

Isochronal temperature sweep measurements (frequency = 1 Hz) were performed on the coacervate samples to measure their phase melting behavior. Figure 10 reveals that when the temperature was increased, the value of the storage modulus (G') decreased because of melting of the junction zones. Junction zones were found to be stable in the temperature range 25−50 °C, and a shoulder gradually appeared at a temperature of ≈68 ± 2 °C; this temperature corresponded to the melting temperature of the junction zones in the coacervate. Another prominent drop in G' value was observed at a temperature of ≈82 ± 2 °C. Theoretical treatment of this melting transition, for coacervate samples, is not trivial mostly due to the absence of any relevant modeling of the problem. However, it may be feasible to adopt models developed for polymer blends in order to understand the phase melting phenomenon occurring in our system. The following discussion is focused on the effect of phase separation kinetics on rheology data.

In a network of transiently connected chains, the shear modulus is proportional to the concentration of intermolecular bonds. The value of the length of elastically active strands, calculated from eq 6, is similar to the characteristic viscoelastic network size (ζ_{el}) estimated from the low frequency shear modulus (G_0). This is a measure of elastic free energy stored per unit volume of a characteristic viscoelastic network of size ζ_{el}. Hence,[43]

$$G_0 \sim k_B T/\zeta_{el}^{\ 3} \tag{6}$$

Experiments reveal that the shear storage modulus of coacervate is weakly dependent on frequency (data not shown) which reaffirms the validity of eq 6. Thus, the typical viscoelastic length scale prevalent in these materials becomes easily accessible from dynamic rheology measurements. The values obtained from the data shown in Figure 10 were $\zeta_{el} \approx 25 \pm 3$ nm in the temperature range 20−70 °C which increased to 35 ± 3 nm when the melting transition temperature (90 °C) was approached. Gelatin coacervates showed a much larger viscoelastic length scale (≈500 nm).[23] This indicates that the internal structures of these two types of coacervates are very different. A second observation was that the signature of the characteristic melting temperature of gelatin gel (≈30 °C) which appeared prominently in gelatin gels and coacervates[23] was completely missing here.

(iii) DSC Studies. The thermal properties were measured using a DSC instrument, (model Perkin-Elmer Pyris 1D). Properly cleaned liquid pans (aluminum) were used, and the instrument was calibrated with cyclohexane. Pyris software supplied by the manufacturer was used to analyze the data. Here, the objective was to determine the melting temperature of coacervates and to correlate the same with the results obtained from rheology. In a DSC experiment, typically 6.5 mg samples were taken in the pan, and the temperature sweep was performed with the heating rate maintained at 1.0 °C/ min. The weak melting behavior observed at $T \approx 65 \pm 3$ °C and the prominent one seen at 90 ± 3 °C could be ascribed to gelling and melting temperatures of the network structures present inside the coacervate phase. It must be recalled that gelatin molecules form

TABLE 1: Summary of Physical Characteristics Describing Various Condensed Phases of Gelatin[a]

Sl no.	parameter/property	gelatin gel	gelatin coacervate	chitosan−gelatin coacervate
1.	mesh size	26 Å (ref 23)	12 Å	(r = 1:10) 12 Å (r = 1:5) 12 Å
2	size of heterogeneity	200 Å (ref 23)	200 Å	(r = 1:10) 215 Å (r = 1:5) 260 Å
3.	first transition temp (DSC)	28 °C (ref 46)	33 °C	71 °C
4.	second transition temp (DSC)			91 °C
5.	first transition temp (rheology)	28 °C (ref 47)	34 °C	64 °C
6.	second transition temp (rheology)			87 °C
7.	viscoelastic feature	viscoelastic	viscous $\eta(\dot{\gamma}) \sim (\dot{\gamma})^{-k}$, $k = 1.4$	viscous $\eta(\dot{\gamma}) \sim (\dot{\gamma})^{-k}$, $k = 0.76$ (r = 1:5)
8.	stoichiometric character		asymmetric (ref 30)	symmetric

[a] The data reported pertain to 20 °C for samples prepared in an aqueous medium (D_2O for SANS experiments). The values listed are representative. The transition temperatures are associated with an uncertainty of ±3 °C and the same with characteristic sizes is ±15% of the listed data, typically.

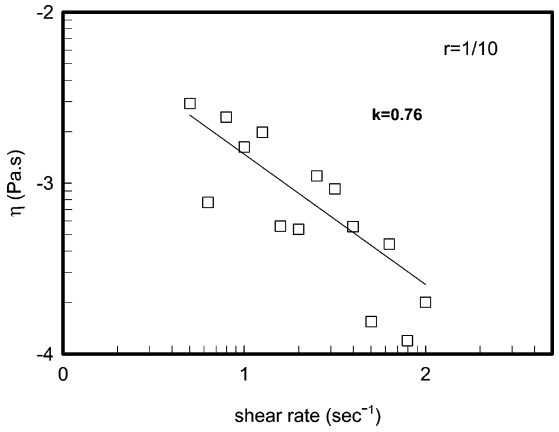

Figure 9. Dependence of viscosity ($\eta(\gamma^{\bullet})$) on shear rate ($\gamma^{\bullet}$) of deformation. The data comfortably fit the power law: $\eta(\gamma^{\bullet}) \sim (\gamma^{\bullet})^{-k}$; $k = 0.76 \pm 0.2$ ($1\ s^{-1} < \gamma^{\bullet} < 100\ s^{-1}$), indicating non-Newtonian behavior and shear induced thinning of the material.

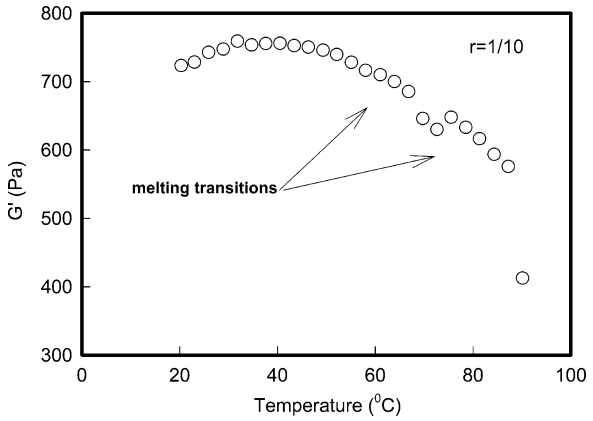

Figure 10. Storage modulus (G', Pa) of coacervate samples plotted as a function of temperature. The temperature ramp was 0.3 °C/ min, a constant oscillation frequency of 1 Hz was used, and a constant strain of 10% was maintained during the experiment. See text for details.

gels comprising interconnected triple helix network structures that melt at[23] ≈28 °C. In the presence of chitosan, it is likely that interpenetrating network structures of gelatin−chitosan molecules are formed that increase the gelation temperature to 65 ± 3 °C and yield a melting temperature close to 90 ± 3 °C. At this stage, it would be premature to give a more explicit description to the melting temperatures observed in Figures 10 and 11. This certainly requires more probing. The corresponding temperatures determined from rheology study were 68 ± 2 and 82 ± 3 °C, respectively, which is not too different from that of DSC results. The area under the endotherm quantifies the

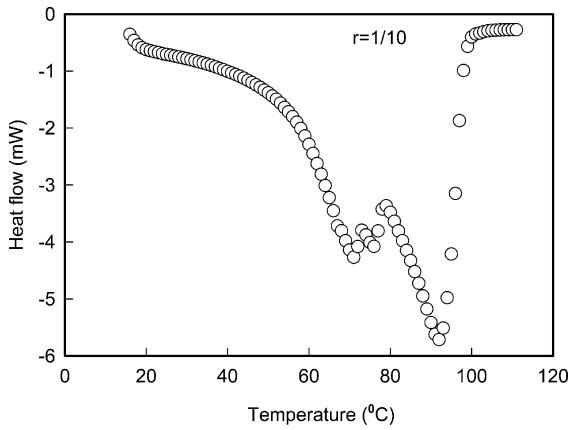

Figure 11. DSC data show the melting transition in coacervates, and it was found that at ≈68 ± 3 °C there is a sharp transition followed by a second transition at ≈82 ± 3 °C. See text for details.

enthalpy of the transition which was much pronounced at the transition occurring at a temperature of ≈90 ± 3 °C. The various melting temperatures pertaining to gelatin gel and coacervate are shown for comparison in Table 1.

IV. Conclusions

It has been shown that a polyelectrolyte, chitosan, and a polyampholyte, gelatin, can undergo associative interactions to form soluble complexes as a precursor to complex coacervation and such a process is predominantly driven by the charge selective patch binding mechanism. It means that, though the net charge on gelatin is positive in the operating pH range, it has a sufficient amount of negatively charged surface to facilitate selective binding with positively charged chitosan molecules overcoming the electrostatic repulsion between positively charged segments of gelatin with that of chitosan. These observations are not at variance with similar results reported earlier.[31−34] In the retention map investigations, the ion-exchange column is aligned at a fixed orientation with respect to the proteins which allows patch binding with ease.[31,34] However, in the bulk, both the polyelectrolyte and polyampholyte follow Brownian dynamics; regardless, it was observed that surface selective binding was enhanced by an increase in the flexibility of the polyion. In our studies, the polyion (chitosan) is likely to have a large persistence length because of the high charge density associated with this molecule. In spite of this, intermolecular soluble complexes could be formed, and the system could be driven toward coacervation following all of the characteristic pathways that are normally associated with the coacervating solution.

We observed an increase in melting temperature of the complex coacervates as compared to that of the individual components. This indicates the presence of physically entangled networks of chitosan and gelatin in the coacervate phase. The viscoelastic response of this phase to external stress is dependent on the specific nature and density of these cross-links. Thus, determination of the degree of helicity present in the coacervate phase will be of significant importance. Gelatin is known to form hydrogels comprising intermolecular triple-helical structures.[44] It is pertinent to ask if similar internal structures prevail inside the coacervate phase. Regardless, it can be concluded that the polymer-rich phase most likely comprises physically cross-linked networks of chitosan and gelatin molecules that are probably interconnected.

It is interesting to observe that gelatin gels and coacervates (simple) share a generality as far as their microscopic internal structures are concerned, which is clearly evident from the data shown in Table 1. Though the characteristic temperatures are different, the rest of the physical signatures are identical. Thus, it would be appropriate to argue that the internal structure of the heterogeneous coacervate material is comprised of cross-linked polymer-rich zones separated by polymer-poor regions having a characteristic viscoelastic length. Such systems are associated with two characteristic relaxation processes: one due to concentration fluctuation and another arising from viscoelastic relaxation. This has been adequately described by models and supported by experiments in the past.[36,45] Thus, the coacervate phase is in a dynamically evolving state that makes this system extremely interesting. The results presented provide significant insight into the distinctive microscopic features of these complex coacervates (chitosan and gelatin) and simple gelatin coacervates. This paper does not answer all of the questions related to the structure of coacervates, yet it makes an attempt to give some foundation to its understanding.

Acknowledgment. A.N.G. is thankful to the council of scientific and industrial research, India, for a senior research fellowship. This work was supported by an IUC-DAEF research grant.

References and Notes

(1) Smith, A. E.; Bellware, F. T. *Science* **1966**, *152*, 362. Smith, A. E. *Science* **1967**, *214*, 1038.
(2) Sato, H.; Nakajima, A. *Polym. J.* **1975**, *7*, 241.
(3) Skepoe, M.; Linse, P. *Macromolecules* **2003**, *36*, 508.
(4) Menger, F. M.; Sykes, B. M. *Langmuir* **1998**, *14*, 4131.
(5) Tsuchida, E.; Abe, K. *Intermacromolecular Complexes*; Springer: Heidelberg, Germany, 1982.
(6) Bungenberg de Jong, H. G. In *Colloid Science*; Kruyt, H. R., Ed.; Elsevier: New York, 1949; Vol. II.
(7) Hinze, H. L.; Armstrong, D. W. *Ordered Media in Chemical Separation*; American Chemical Society: Washington, DC, 1987; Vol. 342.
(8) Xia, J.; Mattison, K. W.; Romano, V.; Dubin, P.; Muhoberac, B. *Biopolymers* **1997**, *41*, 359.
(9) Wang, Y.; Banziger, J.; Filipelli, G.; Dubin, P. L. *Environ. Sci. Technol.* **2001**, *35*, 2608.
(10) Dubin, P.; Gao, J,; Mattison, K. *Sep. Purif. Methods* **1994**, *23*, 1. Wang, Y.; Banziger, J.; Filipelli, G.; Dubin, P. L. *Environ. Sci. Technol.* **2001**, *35*, 2608.
(11) Burgess, D. J.; Carless, J. E. *Int. J. Pharm.* **1985**, *27*, 61.
(12) Kaibara, K.; Okazaki, T.; Bohidar, H. B.; Dubin, P. L. *Biomacromolecules* **2000**, *1*, 100.
(13) Veis, A.; Cohen, J. *J. Phys. Chem.* **1956**, *78*, 6238. Veis, A. *J. Phys. Chem.* **1963**, *65*, 1960. Veis, A. *J. Phys. Chem.* **1961**, *61*, 1798. Veis, A.; Aranyi, C. *J. Phys. Chem.* **1960**, *64*, 1203.
(14) Tainaka, K. *Biopolymers* **1980**, *19*, 1289. Tainaka, K. *J. Phys. Soc. Jpn.* **1979**, *46*, 1899.
(15) Nakajima, A.; Sato, H. *Biopolymers* **1972**, *10*, 1345.
(16) Overbeek, J.; Voorn, M. J. *J. Cell. Comput. Physiol.* **1957**, *49* (Suppl. 1), 7.
(17) Gupta, A.; Bohidar, H. B. *Phys. Rev. E* **2005**, *72*, 011507.
(18) (a) Dubin, P. L.; Rigsbee, D. R.; McQuigg, D. W. *J. Colloid Interface Sci.* **1985**, *105*, 509. (b) Dubin, P. L.; Rigsbee, D. R.; Gans, L. M.; Fallon, M. A. *Macromolecules* **1988**, *21*, 2555. (c) Dubin, P. L.; The, S. S.; McQuigg, D. W.; Chew, C. H.; Gans, L. M. *Langmuir* **1989**, *5*, 89.
(19) Kokufuta, E.; Shimizu, H.; Nakamura, I. *Macromolecules* **1982**, *15*, 1618.
(20) Uragami, T.; Tokura, S. *Material Science of Chitin and Chitosan*; Springer: New York, 2006.
(21) Pezron, I.; Djabourov, M.; Leblond, J. *Polymer* **1991**, *32*, 3201.
(22) Veis, A. *The Macromolecular Chemistry of Gelatin*; Academic Press: New York, 1964.
(23) Mohanty, B.; Aswal, V. K.; Kohlbrecher. Bohidar, H. B. *J. Polym. Sci., Part B* **2006**, *44*, 1653.
(24) Schmitt, C.; Sanchez, C.; Lamprecht, A.; Renard, D.; Lehr, C. M.; de Cruif, C. G.; Hardy, J. *Colloids Surf., B* **2001**, *20*, 267. Sanchez, C.; Mekhloufi, G.; Schmitt, C.; Renard, D.; Robert, P.; Lehr, C. -M.; Lamphret, A.; Hardy, J. *Langmuir* **2002**, *18*, 10323.
(25) Weinbreck, F.; Tromp, R. H.; de Cruif, C. G. *Biomacromolecules* **2004**, *5*, 1437. Weinbreck, F.; Rollema, H. S.; Tromp, R. H.; de Cruif, C. G. *Langmuir* **2004**, *20*, 6389.
(26) Wang, Y.; Li, Y.; Wang, Yu-W.; Lal, J.; Huang, Q. *J. Phys. Chem. B* **2006**, *111*, 515.
(27) Bohidar, H.; Dubin, P. L.; Majhi, P.; Tribet, C.; Jaeger, W. *Biomacromolecules* **2005**, *6*, 1573.
(28) Seyrek, E.; Dubin, P. L.; Tribet, C.; Gamble, E. A. *Biomacromolecules* **2003**, *4*, 273.
(29) Kayitmeyer, A. B.; Shaw, D.; Dubin, P. L. *Macromolecules* **2005**, *38*, 5198.
(30) Mohanty, B.; Bohidar, H. B. *Biomacromolecules* **2003**, *4*, 1080.
(31) Lesins, V.; Ruckenstein. *Colloid Polym. Sci.* **1988**, *266*, 1187.
(32) Gao, J.; Dubin, P. L.; Muhoberac, B. B. *J. Phys. Chem.* **1998**, *102*, 3329.
(33) Park, J. M.; Muhoberac, B. B.; Dubin. P. L.; Xia, J. *Macromolecules* **1992**, *25*, 290.
(34) Kopaciewicz, W.; Rounds, M. A.; Fausnaugh, J.; Regnier, F. E. *J. Chromatogr.* **1983**, *266*, 3.
(35) Manning, G. S. *J. Phys. Chem. B* **1980**, *84*, 1059.
(36) Mohanty, B.; Bohidar, H. B. *Europhys. Lett.* **2006**, *76*, 965.
(37) Aswal, V. K.; Goyal, P. S.; *Curr. Sci.* **2000**, *79*,947.
(38) Thiyagaranjan, P.; Epperson, J. E.; Crawford, R. K.; Carpenter, J. M.; Klippert, T. E.; Wozniak, D. G. *J. Appl. Crystallogr.* **1997**, *30*, 280.
(39) Debye, P.; Bueche, A. M. *J. Appl. Phys.* **1949**, *20*, 518.
(40) deGennes, P. G. *Scaling Concepts in Polymer Physics*, 2nd ed.; Cornell University Press: Ithaca, New York, 1985.
(41) Koberstein, J. T.; Picot, C.; Benoit, H. *Polymer* **1985**, *26*, 673.
(42) Barnes, H. A. *A Handbook of Elementary Rheology*; University of Wales Press: Wales, England, 2000.
(43) Ajji, A.; Choplin, L. *Macromolecules* **1991**, *24*, 5221.
(44) Busnel, J. P.; Morris, E. R.; Ross-Murphy, S. B. *Int. J. Biol. Macromol.* **1989**, *11*, 119. Busnel, J. P.; Ross-Murphy, S. B. *Int. J. Biol. Macromol.* **1988**, *10*, 121.
(45) Edwards, S. F.; Freed, K. F. *J. Phys. C: Solid State Phys.* **1970**, *3*, 739, 750, 760.
(46) Bohidar, H. B.; Jena, S. S. *J. Chem. Phys.* **1998**, *98*, 8970.
(47) Labropoulos, K. C.; Niesz, D. E.; Danforth, S. C.; Keverkidis, P. G. *Carbohydr. Polym.* **2002**, *50*, 393.